



Contents lists available at ScienceDirect

Optik - International Journal for Light and Electron Optics

journal homepage: www.elsevier.com/locate/ijleo

Original research article

An efficient method for scanned images by using color-correction and L_0 gradient minimization

Jing Ji ^{a,b}, Suping Fang ^{a,*}, Qing Xia ^c, Zhengyuan Shi ^c^a Xi'an Jiaotong University, State Key Laboratory of Manufacturing Systems Engineering, Xi'an 710049, China^b Xi'an Jiaotong University Museum, Xi'an Jiaotong University, Xi'an 710049, China^c School of Mathematics and Statistics, Xi'an Jiaotong University, Xi'an 710049, China

ARTICLE INFO

Keywords:

Color correction
Image smoothing
 L_0 Sparsity
Fast solver

ABSTRACT

To improve the quality of scanned image captured by cameras, we propose a novel and efficient method for image processing by using color-correction and L_0 gradient minimization. Our method is divided into two steps. To derive a colorimetric mapping between digital RGB signals and real image values, we use a polynomial model by considering the interrelations among the standard color spaces. A L_0 gradient minimization is used to remove the image noises. Based on the half-quadratic splitting method, an iterative algorithm for our proposed method is developed. The iterative algorithm is easy to implement with the optimal complexity $O(N \log N)$. Our method is particularly beneficial to correct image color and remove image noises. Various tests are presented to demonstrate the robustness and efficiency of our method.

1. Introduction

Images are scanned by the camera into computers for secondary processing and archiving [1–3]. When the equipment starts to work, the reflected light passes through the lens into the scan camera, which can perform optical–electrical conversion. After scanning with the camera and comparing with the image acquisition card, the image information is transferred to the computer for processing and analysis. However, the quality of the obtained image is affected by many factors during the scanning process, such as the light intensity and the optical resolution of the scanner. These factors will change the image tone and bring new noise. Fig. 1(a) and (b) show the exact image and scanned digital image, respectively. As can be seen, there is a deviation between the scanned image and the exact image due to the unsatisfactory external environment. To improve the quality of scanned images, we aims to develop a novel post-processing method by combining a color correction part and a noise removal part. With the color corrected method, the image is corrected as shown in Fig. 1(c). With the noised removal method, the quality of the scanned image is improved as shown in Fig. 1(d).

Generally, the digital camera is firstly used to scan the standard colorimetric card. Then by comparing the values of pixels in the standard colorimetric card and the scanned image, a color transforming map can be established to transform the scanned image to its exact one. Many color correction methods have been developed. Hung [4] proposed a look-up-table model with tetrahedral interpolation techniques to calibrate the pixel color for the electronic imaging devices. This model used a matrix of color patches and developed the interpolations on the assumption of smoothness. Mendes et al. [5] used an adaptive polynomial regression and genetic algorithm, which combined a weighted least square approach indirectly and used for the automatic visual inspection. Hardeberg et al. [6,7] introduced a preprocess of polynomial regression in which a cubic root of RGB values is used. This method applied a

* Corresponding author.

E-mail address: spfang@mail.xjtu.edu.cn (S. Fang).

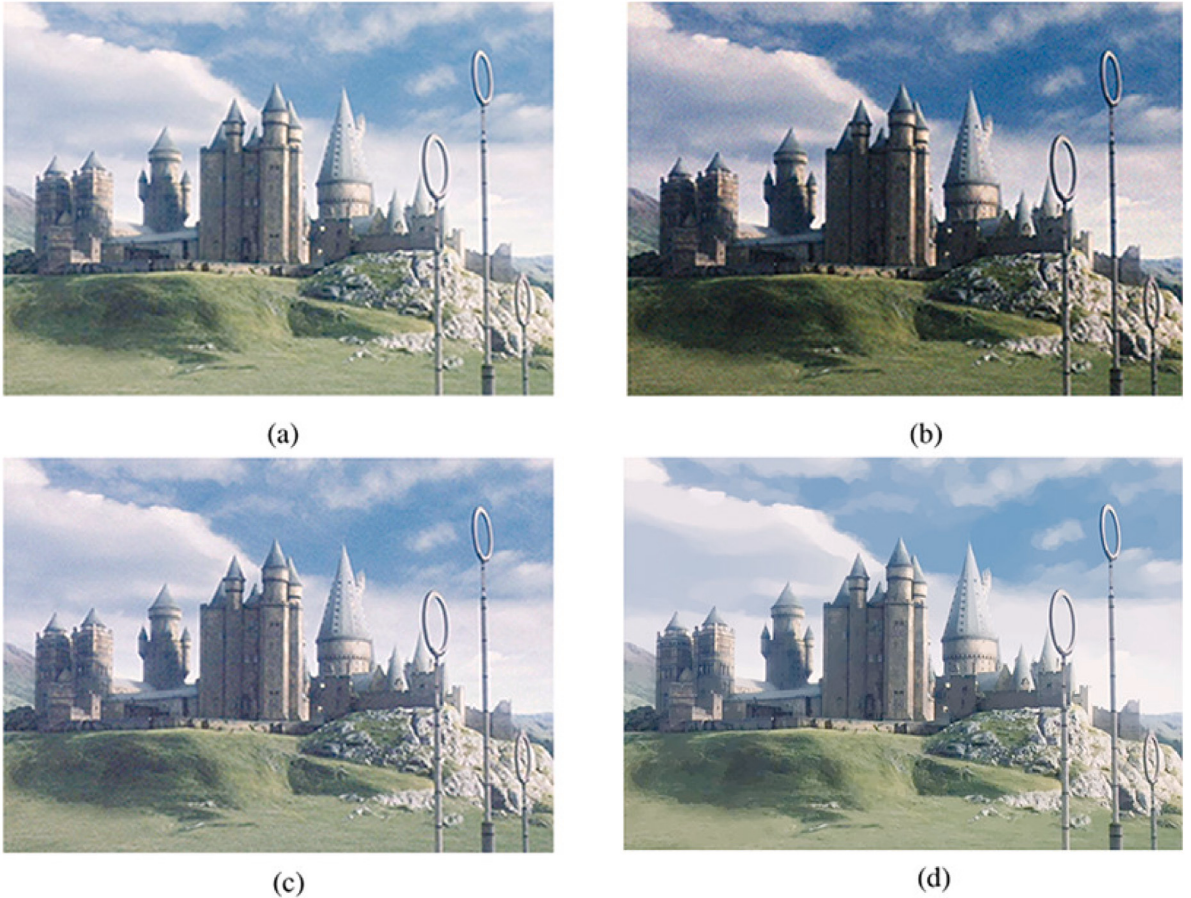


Fig. 1. (a) Exact image. (b) Scanned image by using the line scanning camera. (c) The color corrected image. (d) The noises removal image. (For interpretation of the references to color in this figure legend, the reader is referred to the web version of this article.)

non-linear correction directly to CIELAB space and obtained high quality digital color images. Andersen et al. [8] matched digital RGBs to CIEXYZs in each hue slice of color space with different polynomial transformations. Rizzi et al. [9] proposed an heuristic algorithm, which aimed to model a simplified version of the inner complex behavior of the human visual system and corrected the images tone. Mantiuk et al. [10] analyzed the color reproduction properties in the tone mapping by extending local and global tone mapping operators. Iqbal et al. [11] proposed a low-light image enhancement technique that simultaneously preserves contrast and removes color saturation from an input image. Zibulevsky et al. [12] used L_1 and L_2 norm to solve optimization problem for image denoising. Gu et al. [13] proposed a weighted nuclear norm minimization algorithm for image denoising and demonstrated the great potentials in low level vision applications. Abascal et al. [14] proposed a novel sparse and prior-based algorithm for 3D image denoising, with the additional benefit of being computationally efficient for application to experimental clinical images. Wang et al. [15] used a modified Allen–Cahn equation for smoothing piecewise linear shapes of two-dimensional and three-dimensional objects. Wang et al. [16] proposed an improved filter for color image denoising based on combining the advantages of non-local means filter and bilateral filter.

In this paper, we will propose a novel and efficient method to solve the post-processing problem for the scanned images. The whole system can be divided into two steps. For the first step, we establish a polynomial regression model to correct the original tone of the scanned image. Euclidean distance is used in CIELAB space to evaluate perceptual color differences. We consider the transformation leading to unsatisfactory results between digital RGB values and the standard CIE values. Therefore, the polynomial root terms extension is constructed in our proposed method to further improve the transformation accuracy. For the second step, we use the L_0 gradient minimization to sharpen prominent edges and reduce noises. This iterative method is simple and easy to implement. Various numerical tests will be presented to demonstrate the robustness and efficiency of our method.

The rest of the paper is organized as follows. In Section 2, we will introduce the transformation between digital RGB space, standard RGB space, CIEXYZ space and CIELab space. Then we describe the proposed color corrected method and L_0 -smoothing method. Section 3 introduces our numerical solver for the L_0 optimization problem. In Section 4, various experimental results are given. Conclusion is drawn in Section 5.

2. Methodology

2.1. Color correction of input images

In this section, we consider the polynomial interrelation among the standard CIE color spaces [17,18]. First, the corresponding tristimulus value is defined as a three dimensional vector \mathbf{q} ($\mathbf{q} \in \mathbb{R}^{3 \times 1}$) and three dimensional digital response of devices is defined as ρ ($\rho \in \mathbb{R}^{3 \times 1}$). A simple linear color characterization transformation can be written as $\mathbf{M} \cdot \rho = \mathbf{q}$. Vector ρ can be extended to m dimensions by increasing basis function in polynomial regression. We define P ($P \in \mathbb{R}^{m \times n}, m \ll n$) as a $m \times n$ matrix of vector ρ and Q ($Q \in \mathbb{R}^{3 \times n}$) as the corresponding matrix of vector \mathbf{q} . The mapping relationship between the camera response space and the corresponding tristimulus value space can be represented by $M \cdot P = Q$, where M is the mapping matrix that depends on P and Q . Once the mapping M is obtained, we can transform the scanned image to its real one. However the standard verify the quality of corrected image [19] is to compute the difference between the real color value $[L_1 \ a_1 \ b_1]^T$ and the obtained color value $[L_2 \ a_2 \ b_2]^T$ in CIELAB space as:

$$\Delta E_{ab} = \sqrt{(L_1 - L_2)^2 + (a_1 - a_2)^2 + (b_1 - b_2)^2}. \quad (1)$$

If $\Delta E_{ab} \in [0, 3]$, the quality of color characterization is very good. If $\Delta E_{ab} \in (6, 10]$, its quality is sufficient. Otherwise, its quality is insufficient. Our goal is to find the optimal mapping matrix M keeping the ΔE_{ab} be small. The three dimensional vector in (-) spaces is defined by $\rho_{(-)}$. It is well known that there is a linear mapping from CIE 1931 Standard RGB Colorimetric System (RGB) to the CIE 1931 Standard XYZ Colorimetric System(CIEXYZ) [20]:

$$\rho_{CIEXYZ} = A \cdot \rho_{RGB}, \quad (2)$$

where

$$A = \begin{bmatrix} 2.7689 & 1.7517 & 1.1302 \\ 1.0000 & 4.5907 & 0.0601 \\ 0.0000 & 0.0565 & 5.5943 \end{bmatrix}.$$

The transformation relationship between CIEXYZ space ($\rho_{CIEXYZ} = (X, Y, Z)$) and CIE 1931 Standard Lab Colorimetric System (CIELab) (ρ_{CIELab}) is non-linear [6,7]:

$$\rho_{CIELab} = N \times \left[f\left(\frac{X}{X_n}\right), f\left(\frac{Y}{Y_n}\right), f\left(\frac{Z}{Z_n}\right) \right]^T + V \quad (3)$$

where

$$N = \begin{bmatrix} 0 & 116 & 0 \\ 500 & -500 & 0 \\ 0 & 200 & -200 \end{bmatrix}, \quad V = \begin{bmatrix} -16 \\ 0 \\ 0 \end{bmatrix}, \quad \begin{bmatrix} X_n \\ Y_n \\ Z_n \end{bmatrix} = \begin{bmatrix} 96.42 \\ 100 \\ 82.49 \end{bmatrix} \quad (4)$$

and

$$f(a) = \begin{cases} a^{\frac{1}{3}} & \text{if } a \geq 0.008856 \\ 7.787a + \frac{16}{116} & \text{otherwise.} \end{cases} \quad (5)$$

We have to remark that $7.787a + 16/116 \approx a^{\frac{1}{3}}$, if $a \leq 0.008856$. Therefore, we simplify the piecewise function Eq. (5) to $f(a) = a^{\frac{1}{3}}$. Substituting Eq. (2) into Eq. (5), we have

$$\begin{cases} f\left(\frac{X}{X_n}\right) = \left(\frac{X}{X_n}\right)^{\frac{1}{3}} = \left(\frac{2.7689}{X_n} R + \frac{1.7517}{X_n} G + \frac{1.1302}{X_n} B\right)^{\frac{1}{3}} \\ f\left(\frac{Y}{Y_n}\right) = \left(\frac{Y}{Y_n}\right)^{\frac{1}{3}} = \left(\frac{1.0000}{Y_n} R + \frac{4.5907}{Y_n} G + \frac{0.0601}{Y_n} B\right)^{\frac{1}{3}} \\ f\left(\frac{Z}{Z_n}\right) = \left(\frac{Z}{Z_n}\right)^{\frac{1}{3}} = \left(\frac{0.0000}{Z_n} R + \frac{0.0565}{Z_n} G + \frac{5.5943}{Z_n} B\right)^{\frac{1}{3}} \end{cases}. \quad (6)$$

We assume that there exists a new vector $[(r^*)^{\frac{1}{3}}, (g^*)^{\frac{1}{3}}, (b^*)^{\frac{1}{3}}]^T$ satisfies

$$\begin{bmatrix} \left(\frac{X}{X_n}\right)^{\frac{1}{3}} \\ \left(\frac{Y}{Y_n}\right)^{\frac{1}{3}} \\ \left(\frac{Z}{Z_n}\right)^{\frac{1}{3}} \end{bmatrix} = \begin{bmatrix} \left(\frac{2.7689}{X_n}\right)^{\frac{1}{3}} & \left(\frac{1.7517}{X_n}\right)^{\frac{1}{3}} & \left(\frac{1.1302}{X_n}\right)^{\frac{1}{3}} \\ \left(\frac{1.0000}{Y_n}\right)^{\frac{1}{3}} & \left(\frac{4.5907}{Y_n}\right)^{\frac{1}{3}} & \left(\frac{0.0601}{Y_n}\right)^{\frac{1}{3}} \\ 0.0000 & \left(\frac{0.0565}{Z_n}\right)^{\frac{1}{3}} & \left(\frac{5.5943}{Z_n}\right)^{\frac{1}{3}} \end{bmatrix} \cdot \begin{bmatrix} (r^*)^{\frac{1}{3}} \\ (g^*)^{\frac{1}{3}} \\ (b^*)^{\frac{1}{3}} \end{bmatrix}, \quad (7)$$

where the color characterization transformation can be assumed as

$$[(r^*)^{\frac{1}{3}}, (g^*)^{\frac{1}{3}}, (b^*)^{\frac{1}{3}}]^T = \hat{M} \cdot \hat{\rho}(R^{\frac{1}{3}}, G^{\frac{1}{3}}, B^{\frac{1}{3}})^T. \quad (8)$$

Here, $\hat{\rho}$ is a polynomial regression and \hat{M} is a mapping matrix. Assume that there exists a \check{M} which satisfies

$$\hat{\rho}(R^{\frac{1}{3}}, G^{\frac{1}{3}}, B^{\frac{1}{3}}) = \check{M} \cdot \rho(R^{\frac{1}{3}}, G^{\frac{1}{3}}, B^{\frac{1}{3}}). \quad (9)$$

Let us use $M := \hat{M} \cdot \check{M}$ and define

$$A^* := \begin{bmatrix} (\frac{2.7689}{X_n})^{\frac{1}{3}} & (\frac{1.7517}{X_n})^{\frac{1}{3}} & (\frac{1.1309}{X_n})^{\frac{1}{3}} \\ (\frac{1.0000}{Y_n})^{\frac{1}{3}} & (\frac{4.5907}{Y_n})^{\frac{1}{3}} & (\frac{0.0601}{Y_n})^{\frac{1}{3}} \\ (\frac{0.0000}{Z_n})^{\frac{1}{3}} & (\frac{0.0565}{Z_n})^{\frac{1}{3}} & (\frac{5.5943}{Z_n})^{\frac{1}{3}} \end{bmatrix}, \quad (10)$$

then combining Eqs. (6)–(10), we have

$$S = N \cdot A^* \cdot M \cdot P + V. \quad (11)$$

Here S and P represent the corresponding matrix of vectors ρ_{CIELab} and ρ_{CIERGB} , respectively. For the standard colorimetric card, S is known. By solving Eq. (11) by using the digital RGB value and real image value, we have

$$M = (A^*)^{-1} \cdot N^{-1} \cdot (S - V) \cdot P^T / (P \cdot P^T). \quad (12)$$

Once we obtain the mapping matrix M , we can transform the scanned image to its real one as following steps:

- Step 1: Using Eqs. (11) and (12), we compute S , which is the corresponding matrix of vectors ρ_{CIELab} .
- Step 2: Using Eq. (3), we calculate $\rho_{CIEXYZ}(X, Y, Z)$.
- Step 3: Using Eq. (2), we obtain the real image $\rho_{RGB}(R, G, B)$.

After these three steps, the tone and chromatic aberration of the scanned image can be improved. Next, we will deal with the extra noise during the scanning process.

2.2. L_0 -smoothing with noise image

Beginning with $I(\mathbf{x})$ which is defined as the color corrected image (ρ_{RGB}), we want to obtain the smoothing result $\phi(\mathbf{x})$. We consider the following L_0 gradient regularization version:

$$\min_{\phi} \int_{\Omega} \|(I(\mathbf{x}) - \phi(\mathbf{x}))\|_2^2 + \beta \|\nabla \phi(\mathbf{x})\|_0 d\mathbf{x} \quad (13)$$

where $\|\cdot\|_2$ is the L_2 norm. The term $\|(I(\mathbf{x}) - \phi(\mathbf{x}))\|_2^2$ enforces ϕ to be similar with color corrected I . Let us briefly review the definition of L_0 -norm: if $\phi = 0$, then $\|\phi\|_0 = 0$. Otherwise, $\|\phi\|_0 = 1$. Therefore the term $\|\nabla \phi(\mathbf{x})\|_0$ can reduce the noises and make edges sharpen. It is worth pointing out that L_0 -norm regularized optimization problem is known as computationally intractable. This optimization problem (Eq. (13)) is equivalent minimize the following equation:

$$G = \|(I(\mathbf{x}) - \phi(\mathbf{x}))\|_2^2 + \beta \|\nabla \phi(\mathbf{x}) - \psi(\mathbf{x})\|_2^2 + \lambda \|\psi(\mathbf{x})\|_0. \quad (14)$$

Here we introduce a new parameter ψ in the optimization problem. β is a wight parameter directly controlling the similarity between ψ and the gradient of ϕ . We can divide the optimization problem of G into two equations as:

$$\begin{aligned} G_1 &= \min_{\psi} \lambda \|\psi\|_0 + \beta \|\nabla \phi(\mathbf{x}) - \psi\|_2^2 \quad \text{with a fixed } \phi, \\ G_2 &= \min_{\phi} \|I(\mathbf{x}) - \phi(\mathbf{x})\|_2^2 + \beta \|\nabla \phi(\mathbf{x}) - \psi\|_2^2 \quad \text{with a fixed } \psi. \end{aligned} \quad (15)$$

For Eq. (15), we should consider the definition of $\|\cdot\|_0$ on the optimization problem with fixed ϕ . We define G_1^* as the minimum of Eq. (15). Considering Eq. (15), if $\lambda = 0$, we can obtain the minimum of G_1 by setting $\psi = \nabla \phi$, otherwise we need to analyze the relationship between $\|\nabla \phi(\mathbf{x})\|_2^2$ and λ/β . The relations are summarized as follows:

(1) When $\|\nabla \phi(\mathbf{x})\|_2^2 \geq \lambda/\beta$, we start splitting in the following two situations. In the first situation, by considering $\psi \neq 0$, we can obtain the minimal value G_1^* by setting $\nabla \phi(\mathbf{x}) = \psi$ shown as

$$G_1^*(\psi \neq 0) = \min_{\psi} G_1(\psi \neq 0) = \lambda \|\psi\|_0 + \beta \|\nabla \phi - \psi\|_2^2 = \lambda \|\nabla \phi\|_2^2 \geq \lambda = \min_{\psi} G_1(\psi \neq 0) \quad (16)$$

For the second situation $\psi = 0$, we can obtain

$$G_1^*(\psi = 0) = \min_{\psi} G_1(\psi = 0) = \lambda \|\psi\|_0 + \beta \|\nabla \phi - \psi\|_2^2 = \beta \|\nabla \phi\|_2^2 \geq \lambda = \min_{\psi} G_1(\psi \neq 0) \quad (17)$$

Therefore, we should only let $\nabla \phi = \psi$ to obtain the minimum G_1^* . In conclusion, combining Eqs. (16) and (17), the minimum energy (15) is produced when $\nabla \phi = \psi$.

(2) When $\|\nabla \phi(\mathbf{x})\|_2^2 < \lambda/\beta$, in a similar way we can obtain

$$G_1^*(\psi \neq 0) = \min_{\psi} G_1(\psi \neq 0) = \lambda, \quad (18)$$

and

$$G_1^*(\psi = 0) = \min_{\psi} G_1(\psi = 0) = \beta \|\nabla \phi\|_2^2. \quad (19)$$

Combining Eqs. (18) and (19), we can find $G_1^*(\psi = 0)$ is smaller than $G_1^*(\psi \neq 0)$. The minimum $G_1^* = \beta \|\nabla \phi\|_2^2$ reaches by choosing ψ as 0. In summary, to minimize Eq. (15), we can obtain the following condition:

$$\psi = \begin{cases} \nabla \phi & \text{if } \lambda = 0 \text{ or } \|\nabla \phi\|_2^2 \geq \frac{\lambda}{\beta}, \\ 0 & \text{otherwise.} \end{cases} \quad (20)$$

Eq. (15) is a quadratic function which has a global minimum even by gradient descent with fixed ψ :

$$-\phi + \beta \Delta \phi = -I + \beta \nabla \cdot \psi \quad (21)$$

3. Numerical solver

We employ the fast scheme with the Fourier-spectral method [21–23]. We assume that there are $N_x \times N_y$ pixels on a 2D image, where N_x and N_y are even integers. Let $x_m = (2m - 1)/2$, $y_n = (2n - 1)/2$, for $1 \leq m \leq N_x$, $1 \leq n \leq N_y$. Furthermore, let ϕ_{mn}^s be an approximation of $\phi(x_m, y_n, s)$, where s is the iterative step. The discrete cosine transform $\hat{\phi}_{pq}^s$ for $p = 1, \dots, N_x$, $q = 1 \dots, N_y$ is defined as

$$\hat{\phi}_{pq}^s = \alpha_p \beta_q \sum_{m=1}^{N_x} \sum_{n=1}^{N_y} \phi_{mn}^s \cos(x_m \pi \xi_p) \cos(y_n \pi \eta_q),$$

where

$$\alpha_p = \begin{cases} \sqrt{1/N_x}, & p = 1 \\ \sqrt{2/N_x}, & 2 \leq p \leq N_x \end{cases} \quad \text{and} \quad \beta_q = \begin{cases} \sqrt{1/N_y}, & q = 1 \\ \sqrt{2/N_y}, & 2 \leq q \leq N_y \end{cases}$$

The variables ξ_p and η_q are defined as $\xi_p = (p - 1)/N_x$ and $\eta_q = (q - 1)/N_y$, respectively. The inverse discrete cosine transform is

$$\phi_{mn}^s = \sum_{p=1}^{N_x} \sum_{q=1}^{N_y} \alpha_p \beta_q \hat{\phi}_{pq}^s \cos(\xi_p \pi x_m) \cos(\eta_q \pi y_n). \quad (22)$$

It is easy to solve ψ^{s+1} from ϕ^s and β^s by using Eq. (20) as

$$\psi^{s+1} = \begin{cases} \nabla \phi^s & \|\nabla \phi^s\|_2^2 \geq \frac{\lambda}{\beta^s}, \\ 0 & \text{otherwise.} \end{cases} \quad (23)$$

Once ψ^{s+1} is obtained, we find that the Eq. (21) for the ϕ at the step ($s + 1$):

$$-\phi_{mn}^{s+1} + \beta^s \Delta \phi_{mn}^{s+1} = -I_{mn} + \beta^s \nabla \cdot \psi_{mn}^{s+1}. \quad (24)$$

Thus, Eq. (24) can be transformed into the discrete cosine space as follows:

$$-(1 + \beta^s)[(\xi_p \pi)^2 + (\eta_q \pi)^2] \hat{\phi}_{pq}^{s+1} = -\hat{I}_{pq} + i \beta^s (\xi_p \pi + \eta_q \pi) \hat{\phi}_{pq}^s$$

Here $i = \sqrt{-1}$ is a complex number and we have employed the discrete cosine transform for the Laplacian and divergence operators, which are defined as

$$\Delta \hat{\phi}_{pq} = -((\xi_p \pi)^2 + (\eta_q \pi)^2) \hat{\phi}_{pq} \text{ and } \nabla \cdot \hat{\psi}_{pq} = i(\xi_p \pi + \eta_q \pi) \hat{\psi}_{pq}.$$

Furthermore, \hat{I}_{pq} and $\hat{\psi}_{pq}$ denote the discrete cosine transform of I_{mn} and ψ_{mn} . Therefore, we obtain the following discrete cosine transform

$$\hat{\phi}_{pq}^{s+1} = \frac{\hat{I}_{pq} - i \beta^s (\xi_p \pi + \eta_q \pi) \hat{\phi}_{pq}^s}{1 + \beta^s (\xi_p \pi)^2 + \beta^s (\eta_q \pi)^2}. \quad (25)$$

The corresponding function ϕ_{mn}^{s+1} can be computed based on Eq. (22). The outline of the main procedure in one time step is as follows:

- Step 1: Initialize ϕ^0 and λ , $\beta = \beta^0$.
- Step 2: Solve ψ^{s+1} from ϕ^s and β^s by using Eq. (23).
- Step 3: Solve ϕ^{s+1} from ψ^{s+1} by using Eqs. (22) and (25).
- Step 4: Update $\beta^{s+1} = \kappa \beta^s$, where κ is larger than 1 to make β increase with each iteration.

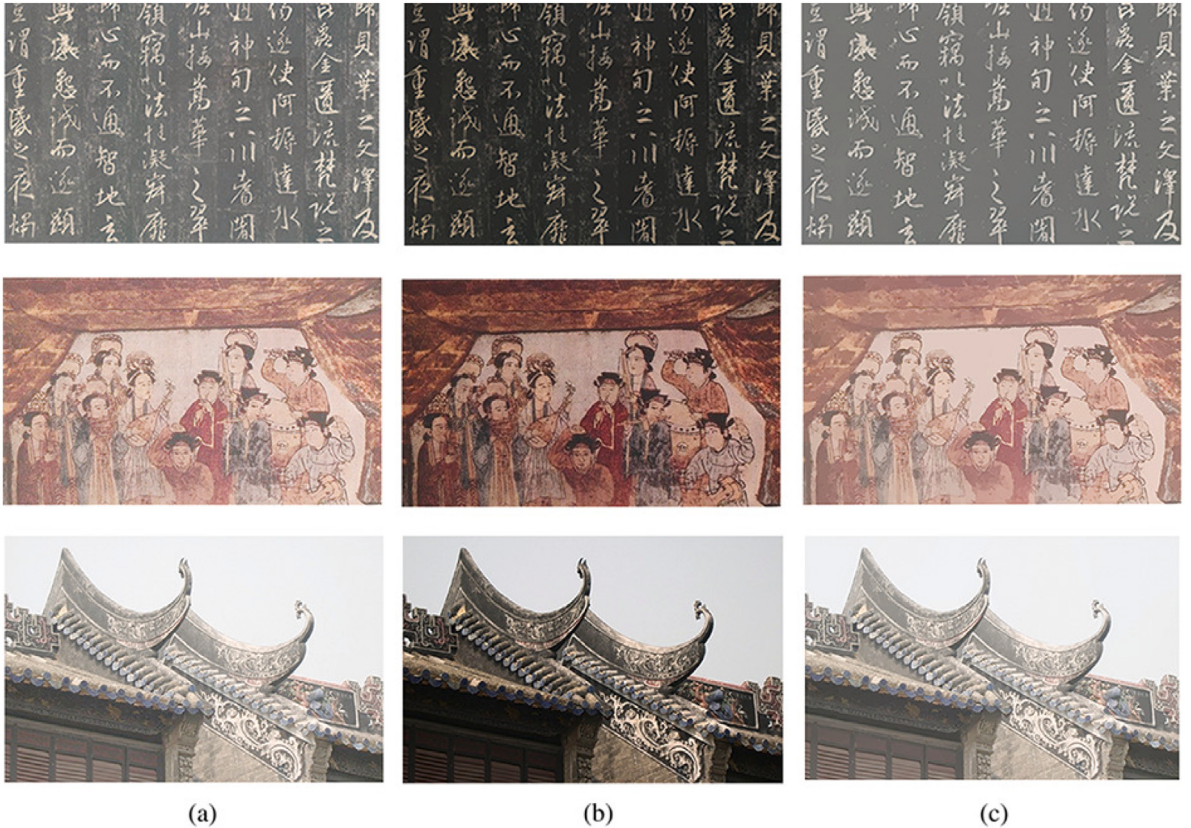


Fig. 2. Color correction of our proposed method. (a) Original image. (b) Digital image captured by camera. (c) Our results. (For interpretation of the references to color in this figure legend, the reader is referred to the web version of this article.)

The main contributions of the proposed method include the following: (i) The proposed method can improve the quality of scanned images without artificial noises because it uses the color-correction and l_0 gradient minimization. (ii) The proposed numerical method in Eqs. (23) and (25) can achieve fast convergence, since our algorithm consists of two explicit evaluations of the closed-form solutions and one implicit Poisson type equation solver. (iii) For the linear equation, their computational complexities are $O(N)$, where N is the size of the mesh grid. For the implicit Poisson type equation solver, we apply a fast discrete cosine transform method with a computational complexity of $O(N \log N)$. Our proposed numerical scheme can be straightforwardly applied to GPU-accelerated DCT implementation that performs up to many times faster than CPU-only alternatives. (iv) The proposed algorithm is simple to implement.

4. Experimental results

In this section, we present numerical results on various synthetic and real images. Fig. 2 shows the cultural relics images. Due to the long preservation time of cultural relics, the difficulty of scanning increases and the brightness and saturation of scanned images decreases as shown in Fig. 2(b). Comparing with Fig. 2(a), our proposed method has performed well in relics color correction as shown in Fig. 2(c). Here, we choose $\beta = 0.02$ and $\kappa = 2$.

To verify the performance of our method, we tested our method with the public data and carried out camera experiments under both ideal and actual light sources. For each set of data, we compared the results of our proposed method with other methods mentioned. The parameters for evaluating the method performance include the mean ΔE_{ab} color difference for all color samples ΔE_{ab} , the maximum ΔE_{ab} color difference ΔE_{max} , the mean error of each color attribute ΔL , Δa , Δb , the maximum error of each color attribute ΔL_{max} , Δa_{max} , Δb_{max} . We consider two data sets. One data set is obtained from the AGFA Arcus II scanner with the AGFA IT8.7/2 color chart. This data set is given in the appendix of the literature [6] proposed by Hardeberg. The other data set is obtained under the ideal light source. Here Nikon D200 camera is applied to capture the image of the X-Rite IT8.7/2 color checker which is positioned in the ColorSpace cabinet and lit by the D65 metamere illuminant.

Tables 1 and 2 show the results obtained by using the methods with RGB–CIEXYZ [24], RGB–CIELAB [25], Hardeberg [6], and our method on the two mentioned data sets. Observing these results, we can see that the direct transformation from digital RGB values to CIELAB space does not provide better results than that from digital RGB values to CIEXYZ space, instead, the results get

Table 1
Data given in the literature experiment results.

Model type	$\overline{\Delta E}$	ΔE_{max}	$\overline{\Delta L}$	ΔL_{max}	$\overline{\Delta a}$	Δa_{max}	$\overline{\Delta b}$	Δb_{max}
RGB-CIEXYZ [24]	4.841	22.939	1.276	3.715	2.782	20.932	3.135	15.354
RGB-CIELAB [25]	22.270	49.111	15.310	34.052	8.422	37.251	9.056	40.062
Hardeberg [6]	5.652	23.961	3.241	11.345	2.234	23.304	2.987	12.645
Our method	1.0130	4.7816	0.3417	2.5473	0.5691	3.3129	0.5913	3.3891

Table 2
Ideal light source experiment results.

Model type	$\overline{\Delta E}$	ΔE_{max}	$\overline{\Delta L}$	ΔL_{max}	$\overline{\Delta a}$	Δa_{max}	$\overline{\Delta b}$	Δb_{max}
RGB-CIEXYZ [24]	4.4162	12.4252	1.7173	7.0779	2.5783	9.0875	2.4828	10.3337
RGB-CIELAB [25]	6.5634	14.4275	3.6462	9.5623	4.0434	9.1865	4.5145	12.6367
Hardeberg [6]	4.1482	10.5636	1.2825	6.7647	2.4636	8.5632	2.2413	9.3883
RPCC [26]	4.5687	12.9247	1.8975	7.5459	2.6586	9.1158	2.5048	10.7479
Our method	2.2016	8.9461	1.1057	4.4196	0.9728	5.5157	1.2968	6.9315

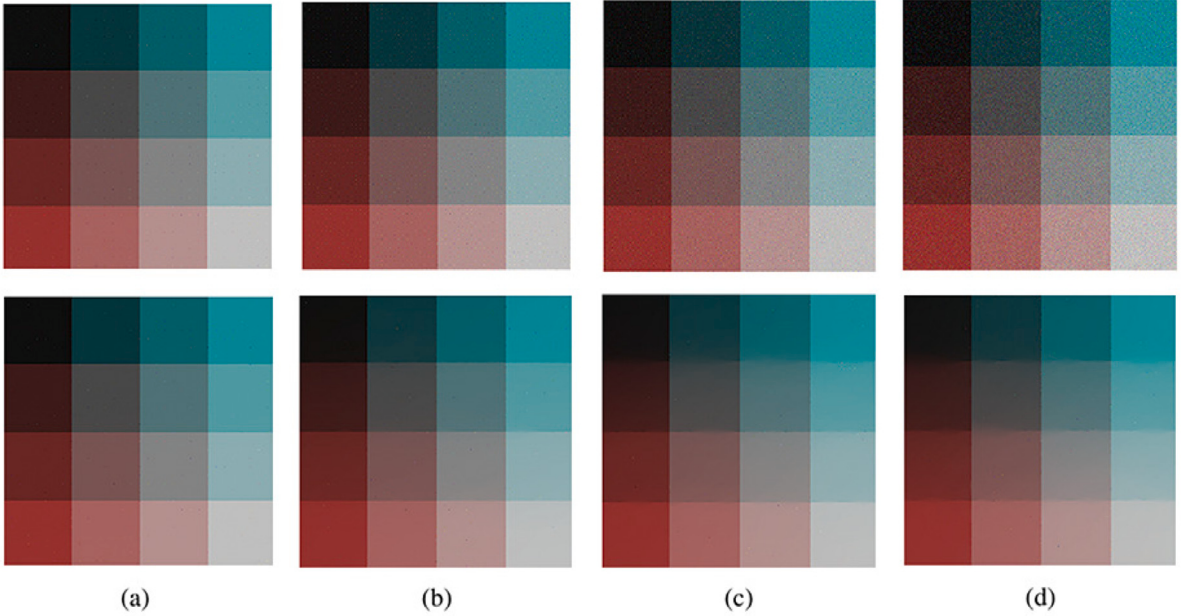


Fig. 3. The top row shows original image with Gaussian noise which expectation is 0 and variance is 0.01. The bottom row shows the denoising results with our method. From (a) to (d), the proportions of noise in the images are 1%, 5%, 15% and 25%, respectively.

worse. This is because the conversion from CIEXYZ to CIELAB is non-linear, involving a cubic root function. But in our method, the color conversion is derived reversely considering the nature of color space transformations, so clearly better results are obtained.

In the top of Fig. 3(a)–(d), we add the Gaussian noises with 1%, 5%, 15% and 25% into a synthetic image acquisition card, respectively. The added noise satisfies the Gaussian distribution with expectation of 0 and variance of 0.01. The given probability $r\%$ means setting a fraction of $r\%$ randomly selected pixels to noises. The bottom row shows the denoising results with our method. Here, we choose the interface parameter $\beta = 0.005, 0.01, 0.015$, and 0.015 , $\kappa = 4.5, 4, 2.4$, and 2 , respectively. We can see that our proposed method successfully remove the noises of the images. Furthermore, as shown in Fig. 3(a–c), our method can keep the sharpen edge when the noise is small. While the too higher noise leads the edges be over-smooth.

Fig. 4 shows the results comparison with different norms in energy function with bronze ware image. Fig. 4(a) is the original image with Gaussian noise. From Fig. 4(b–d), we use L_0 , L_1 and L_2 norms in the energy function minimization (Eq. (13)), respectively. In our algorithm, we choose $\beta = 0.01$ and $\kappa = 1.85$. Note that we have used an iterated soft-thresholding algorithm for L_1 as introduced in [27]. It is worth pointing out that L_1 and L_2 norms homogenizes the noise in the image which makes the original image blurred. However, L_0 norm can enhance the contrast of image and suppress low-amplitude details.

In Fig. 5, we present a synthetic image and a real image with noises in first and second rows, respectively. In order to ignore the influence of iteration step, we set $\kappa = 2$ for every image. The denoising results parameters $\beta = 0.02, 0.04$, and 0.08 are used in Fig. 5(b–d), respectively. As can be observed, the noises of the images will be reduced and the texture will be improved gradually.

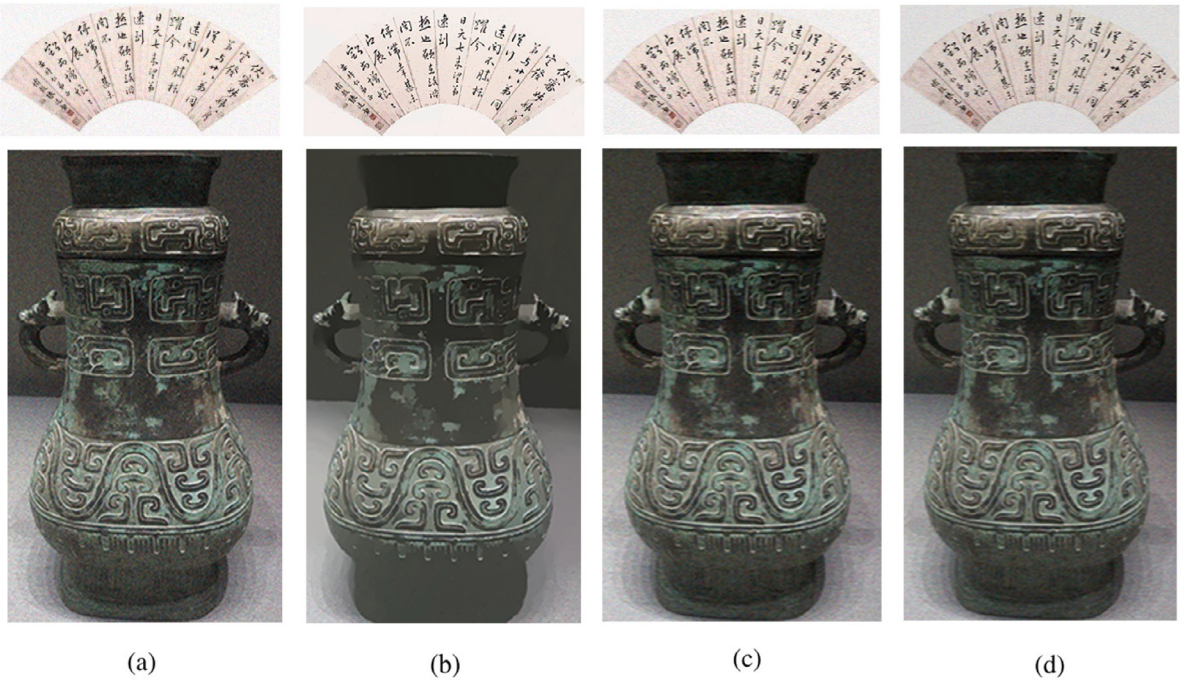


Fig. 4. Results with different norms in energy function with bronze ware image. (a) Initial image with Gaussian noise. (b)–(d) Results of minimization energy function with L_0 , L_1 and L_2 norm.

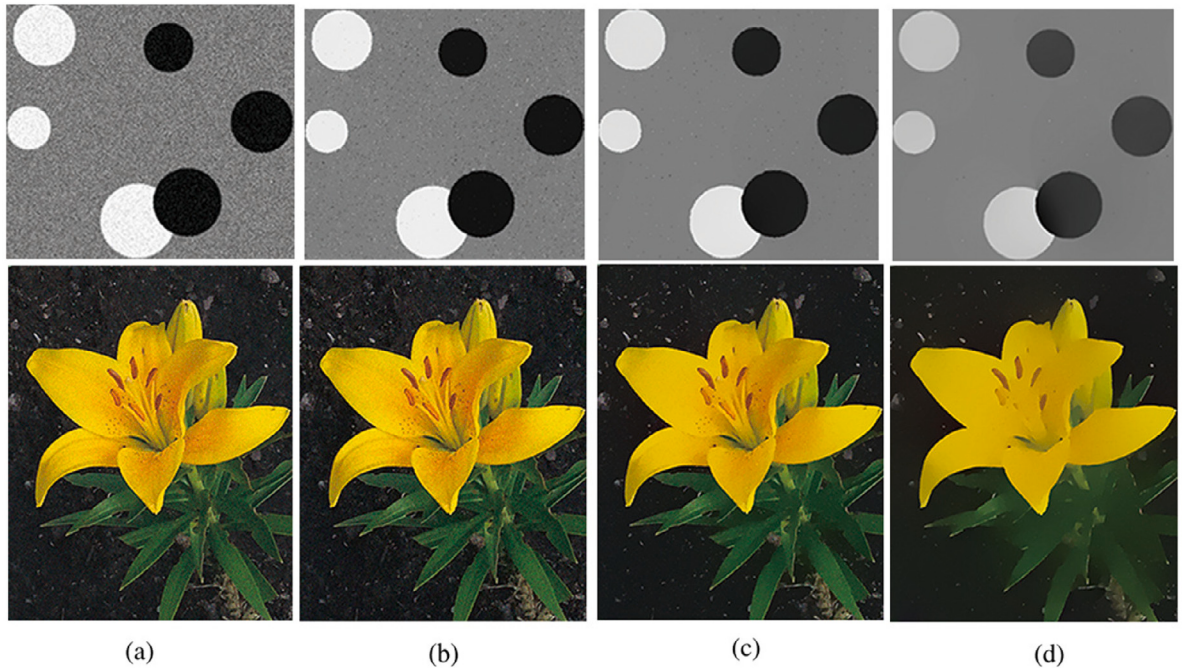


Fig. 5. Result comparison with quantization and denoising. (a) The image with noise. (b-d) The denoising parameters are $\beta = 0.02, 0.04$ and 0.08 , respectively. Here $\kappa = 2$ is fixed.

For the synthetic image, because there is no influence of texture, Fig. 5(d) with $\beta = 0.08$ has a good result. For the real image, Fig. 5(c) has a better result because it is closer to the authentic scene.

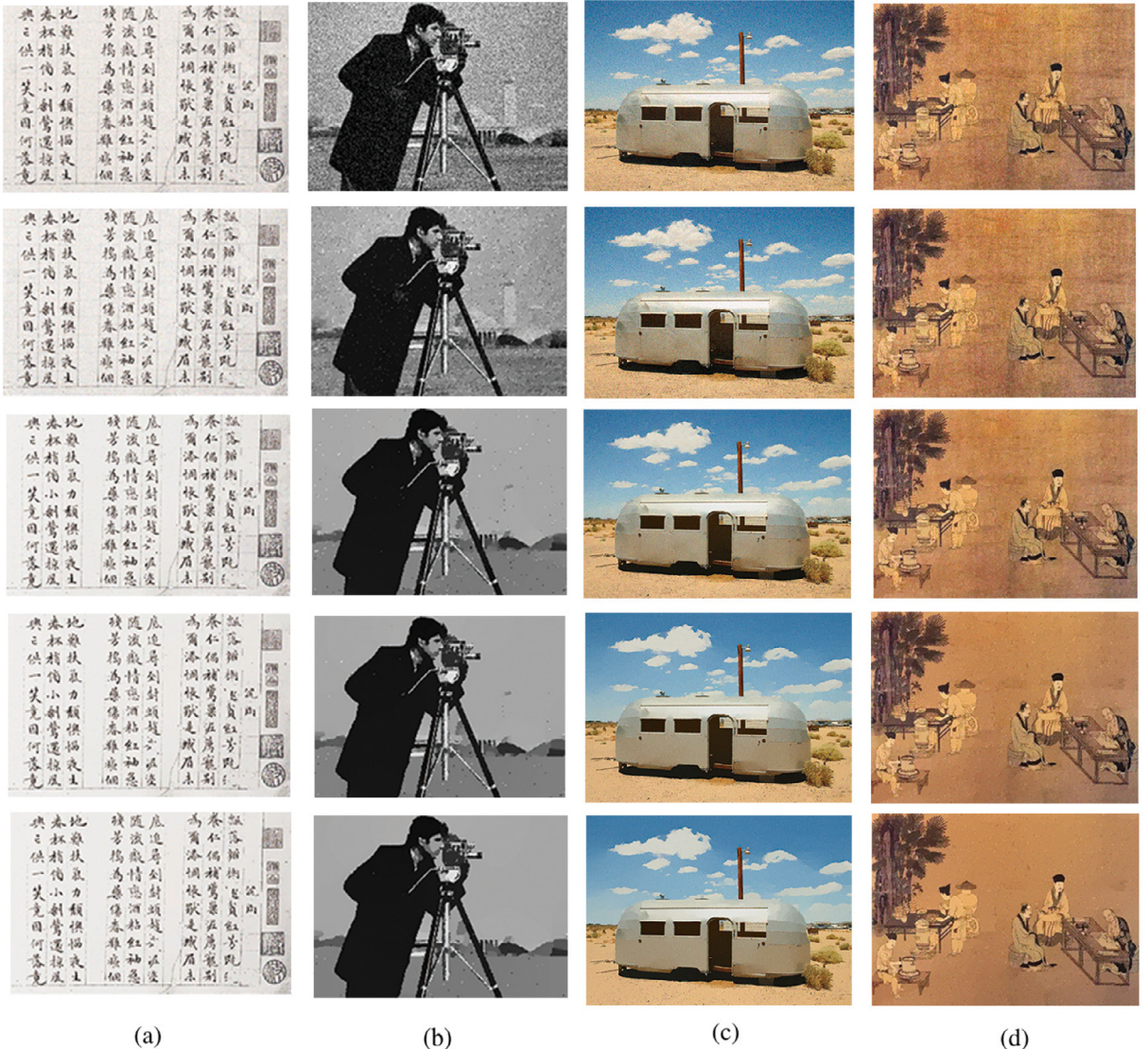


Fig. 6. Comparison results by different iterations with $\beta = 0.02$. (a) is the original images with gaussian noise. From left to right, we use hand-writing image, gray-scale image, color image and real culture relic image to test the effect of our method, respectively. From (b) to (e), the results are the images with 10 iterations ($\kappa = 4.5$), 30 iterations ($\kappa = 1.65$), 50 iterations ($\kappa = 1.35$) and 70 iterations ($\kappa = 1.25$), respectively. (For interpretation of the references to color in this figure legend, the reader is referred to the web version of this article.)

Fig. 6 shows the comparison results by different iterations with fix $\beta = 0.02$, which shows our proposed method performed well by increasing iterations with fix β . In this figure, we use various types of images, which are hand-writing image, gray-scale image, color image and real culture relic image, respectively, to verify the robustness of proposed method. From (b) to (e), we choose κ as 4.50, 1.65, 1.35 and 1.24, which represent 10 iterations, 30 iterations, 50 iterations and 70 iterations, respectively. As can be seen in **Fig. 6(d)** and (e), our method has eliminated most of noise and sharpen the edge. Meanwhile, choosing adaptive β can lead to better results.

In the final test, we use the several real scanned images as shown in **Fig. 7**. From **Fig. 7(a)**, we correct the color of the images and get the clear results in **Fig. 7(b)**, which have even color character and the contrast is obvious. Here we choose the smooth parameter $\beta = 0.01$, and run the simulation up to 20 iterations to get the denoising ancient Egypt in **Fig. 7(c)**. For denoising ancient Roman fresco in **Fig. 7**, we choose $\beta = 0.01$ and $\kappa = 1.65$. In **Fig. 7(c)**, the contents of the cultural relics have been highlighted and the noises are reduced, except for the damaged parts. As can be seen, our algorithm disposes the relics images well.

Finally, we show the performance of all test problems. We calculate the average CPU time per iteration (total CPU time over total iterations) and fit the curve with images size as shown in **Fig. 8**. Here, the linear fitting is done using the MATLAB function polyfit.

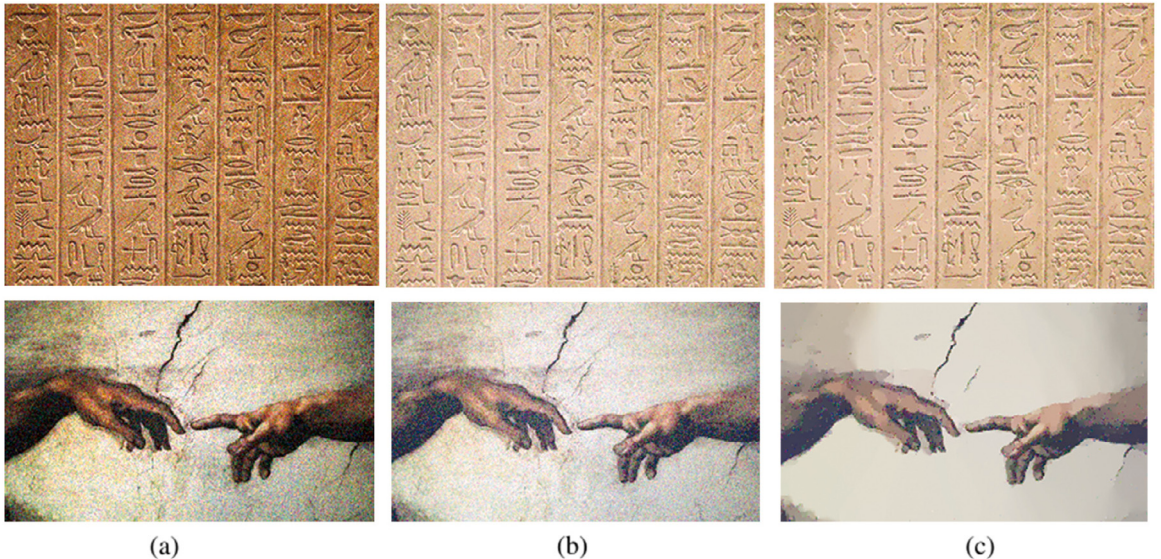


Fig. 7. Full processing of real scanned images with hieroglyphically characters in ancient Egypt and ancient Roman fresco. (a) are the scanned images with affected tone and noise. (b) are the results of color corrected images with noise. (c) are the final results with corrected color and noise. (For interpretation of the references to color in this figure legend, the reader is referred to the web version of this article.)

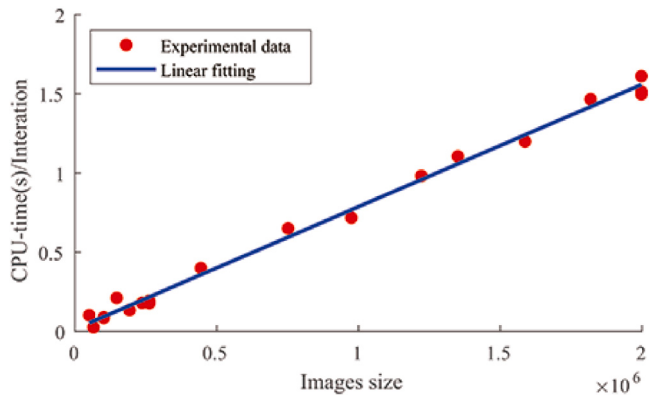


Fig. 8. Experimental data and linear fitting average CPU time per iteration versus image size.

It can be seen that the convergence rate of the computational cost is linear with respect to images size. Therefore, our method is simple and fast.

5. Conclusion

In this paper, we have presented a novel robust and efficient method for image processing using color-correction and L_0 gradient minimization, which gives an obvious improvement in color characterization accuracy and removes noise of the images. Our method can be improved in several ways. First, we can extend the polynomial root terms to further improve the transformation of color correction accuracy. The results presented in this paper show that this algorithm outperforms linear regression and offers a significant improvement over polynomial models when the exposure/scene irradiance varies. The polynomial root terms extension is constructed in our proposed method to further improve the transformation accuracy. Then, automatically adapting parameters of L_0 minimization can get sharper features and eliminate noises. Unlike other denoising methods with L_1 or L_2 norm, our method can remove low-amplitude pixels and globally preserve and enhance salient edges, even if they are boundaries of very narrow objects. This iterative algorithm is easy to implement and computational efficient. Various tests are presented to demonstrate that our method is robust and produces good image processing results.

Declaration of competing interest

The authors declare that they have no known competing financial interests or personal relationships that could have appeared to influence the work reported in this paper.

Acknowledgments

This work is supported by National Natural Science Foundation of China (No. 11631012, 11771348) and the Fundamental Research Funds for the Central Universities, China (No. XTR042019005).

References

- [1] A. Molada-Tebar, J.L. Lerma, A. Marques-Mateu, Camera characterization for improving color archaeological documentation, *Color Res. Appl.* 43 (14) (2017) 47–57.
- [2] M. Barni, A. Pelagotti, A. Piva, Image processing for the analysis and conservation of paintings: opportunities and challenges, *IEEE Signal Proc Mag.* 22 (5) (2005) 141–144.
- [3] R. Parry, Digital heritage and the rise of theory in museum computing, *Mus. Manag. Curator.* 20 (4) (2005) 333–348.
- [4] P.C. Hung, Colorimetric calibration in electronic imaging devices using a look-up table model and interpolations, *Electronic Imag.* 2 (1) (1993) 53–61.
- [5] L. Mendes, P. Carvalho, Adaptive polynomial regression for colorimetric scanner calibration using genetic algorithms, in: Proceedings of the IEEE International Workshop on Intelligent Signal Processing, 2005, pp. 22–27.
- [6] J.Y. Hardeberg, *Acquisition and Reproduction of Colour Images: Colorimetric and Multispectral Approaches* (Doctoral Thesis), 1999.
- [7] J.Y. Hardeberg, F. Schmitt, I. Tastl, H. Brettel, J.P. Crettez, Color management for color facsimile, in: Proc. IST and SIDs 4th Color Imaging Conf.: Color Science, Systems and Applications, Scottsdale, 1996, pp. 108–113.
- [8] C.F. Andersen, J.Y. Hardeberg, Colorimetric characterization of digital cameras preserving hue planes, in: Proc. 13th Color Imag. Conf., 2005, pp. 141–146.
- [9] A. Rizzi, C. Gatta, D. Marini, A new algorithm for unsupervised global and local color correction, *Pattern Recognit. Lett.* 24 (2003) 1663–1677.
- [10] R. Mantiuk, R. Mantiuk, A. Tomaszevska, W. Heidrich, Color correction for tone mapping, *Comput Graph Forum.* 28 (2009) 193–202.
- [11] M. Iqbal, S.S. Ali, et al., Color and white balancing in low-light image enhancement, *Optik* 209 (2020).
- [12] M. Zibulevsky, M. Elad, L_1 - L_2 Optimization in signal and image processing, *IEEE Signal Proc Mag.* 27 (3) (2010) 76–88.
- [13] S. Gu, L. Zhang, W. Zuo, X. Feng, Weighted nuclear norm minimization with application to image denoising, in: Proc. IEEE Conf. Comput. Vis. Pattern Recognit., Jun. 2014, pp. 2862–2869.
- [14] J.F.P.J. Abascal, S. Si-Mohamed, P. Douek, C. Chappard, F. Peyrin, A sparse and prior based method for 3D image denoising, HAL-02056591, 2019.
- [15] J. Wang, Y. Li, Y. Choi, C. Lee, J. Kim, Fast and accurate smoothing method using a modified Allen-Cahn equation, *Comput. Aided Des.* 120 (2020) 102804.
- [16] G. Wang, Y. Liu, W. Xiong, Y. Li, An improved non-local means filter for color image denoising, *Optik.* 173 (2018) 157–173.
- [17] L.L. Weatherall, B.D. Coombs, Skin color measurements in terms of CIELAB color space values, *J. Inverst. Dermatol.* 4 (99) (1992) 468–473.
- [18] C. Connolly, T. Fleiss, A study of efficiency and accuracy in the transformation from RGB to CIELAB color space, *IEEE T. Image Process.* 7 (6) (1997) 1046–1048.
- [19] A. Abrardo, V. Cappellini, M. Cappellini, A. Mecocci, Art-works colour calibration using the VASARI scanner, in: Proc. 4th IS & T/SID Color Imaging Conf., vol. 94, 1996.
- [20] S. Süsstrunk, R. Buckley, S. Swen, Standard RGB color spaces, *Color Imag Conf* 1 (1999) 127–134.
- [21] G. Sheng, T. Wang, Q. Du, K.G. Wang, Z.K. Liu, L.Q. Chen, Coarsening kinetics of a two phase mixture with highly disparate diffusion mobility, *Commun. Comput. Phys.* 8 (2010) 249–264.
- [22] Y. Li, J. Kim, Multiphase image segmentation using a phase-field model, *Comput. Math. Appl.* 62 (2011) 737–745.
- [23] Y. Li, J. Kim, An unconditionally stable hybrid method for image segmentation, *Appl. Numer. Math.* 82 (2014) 32–43.
- [24] G. Hong, M.R. Luo, P.A. Rhodes, A study of digital camera colorimetric characterization based on polynomial modeling, *Color Res. Appl.* 26 (1) (2001) 76–84.
- [25] B. Sun, H. Liu, S. Zhou, W. Li, Evaluating the performance of polynomial regression method with different parameters during color characterization, *Math. Probl. Eng.* 2014 (1) (2014) 1–7.
- [26] G.D. Finlayson, M. Mackiewicz, A. Hurlbert, Color correction using root-polynomial regression, *IEEE T. Image. Process.* 24 (5) (2015) 1460–1470.
- [27] M. Schmidt, G. Fung, R. Rosales, Fast optimization methods for L_1 regularization: a comparative study and two new approaches, in: Proc. 18th European Conf. on Machine Learning (ECML), 2007, Warsaw, Poland, pp. 286–297.